Probability of Helicopter Blade Flash Interception in Search Radar

R.J. Berndt, W.A.J. Nel, *Senior Member, IEEE,* M.Y. Abdul Gaffar and D.W. O'Hagan, *Member, IEEE*

***Abstract*—Helicopter main rotor blade flashes in radar measurements are an oft-used feature for target classification. While focus is often placed on being able to detect them, little attention has been given to what is required to ensure that they are reliably and persistently intercepted. Using mathematical analysis and simulation, this paper explores the probability of helicopter blade flash interception in search radar. The effects of radar antenna azimuth beamwidth, scan rate, and waveform on the average probability of intercept for two-bladed helicopter blade flashes (a worst-case scenario) are examined. The results presented provide an upper bound on achievable flash detection performance and can be used to understand and optimize the performance of helicopter classification modes.**

***Index Terms*—Probability of Intercept (PoI), helicopter blade flash, radar, PRF, dwell, scan, pulse train, Non-cooperative Target Recognition (NCTR), classification.**

I. Introduction

One of the most commonly suggested and used features in radar measurements of helicopters is main rotor blade flashes. The topic has received significant attention in literature over more than three decades. Early mathematical models of blade returns were produced by Schneider [1] and Martin and Mulgrew [2]. Numerous subsequent studies such as [3]–[7] have made use of measurements to validate blade flashing models. Another avenue of research has focused on the exploitation of blade modulation for the classification and identification of helicopters. Examples include time domain [8], [9], time-frequency [10], [11] and sparse signal representation [12], [13] approaches.

The exploitation of blade flashes in radar measurements presupposes that they have been intercepted. This is potentially a limiting factor in search radar. As Misiurewicz notes in [5], the interception of blade flashes in a single scan are rare under the normal operating conditions of a rotating antenna. Interception also places an upper bound on the achievable detection performance. Despite this, it has only received cursory attention in literature.

Interception of blade flashes in pulse-Doppler search radar depends mainly on two radar parameters. Firstly, the Pulse Repetition Interval (PRI) must be short enough such that a blade flash cannot occur between two successive pulses without being intercepted. Secondly, the dwell time on target must be long enough such that at least one blade flash must occur during a dwell. Misiurewicz [9] provides requirements on the minimum values of PRI and dwell time on target to guarantee a blade flash intercept. When these requirements are not met, simplifying independence assumptions are made to calculate the cumulative probability of flash interception after a certain number of consecutive scans. Likewise, Tait [14] provides requirements on PRI and target dwell to ensure interception and suggests that the cumulative probability over several short dwells can be used to obtain reasonable interception performance. Olsen et al. [15] also provide a discussion on blade flash interception, however, their work was limited to the requirements on pulse duration and PRI to guarantee intercept. While the requirements to guarantee intercept have been well covered [9], [14], [15], insufficient analysis has been conducted for the case when these requirements are not met. The contributions of this paper are focused on addressing this. The insights can be used to better understand the trade-offs and limitations associated with the use of helicopter blade flashing in search radar.

The remainder of this paper is structured as follows. Section II frames the probability of intercept problem as one concerning the interception of pulse trains and outlines some assumptions made in the analysis. In Section III, the concept of helicopter main rotor blade flashing is introduced and equations developed to specify the associated parameters. Thereafter, Section IV introduces the blade flash interception problem and discusses the minimum requirements on PRI and target dwell time to guarantee interception. Thereafter, Section V discusses the two pulse PoI problem and presents PoI results related to radar waveform (i.e. PRI) and scanning. In Section VI, the three pulse train PoI problem is analyzed and results presented when radar waveform and scanning are simultaneously accounted for. Finally, conclusions are drawn in Section VII.

II. Problem Formulation

Helicopter blade flash interception can be modeled as a pulse train interception problem. Specifically, the periodic processes involved, namely radar scanning or rotating, helicopter blade flashing and radar waveform can be modeled as pulse trains. This is shown in Fig. 1. Note that the starting phases (ϕ), are defined for convenience from the falling edge of a pulse. The pulse widths and periods are derived from designed radar and helicopter parameters and are assumed to be consistent. Note that this means the analysis is only

R.J. Berndt is with the Council for Scientific and Industrial Research, Pretoria, South Africa, and the Department of Electrical Engineering, University of Cape Town, Cape Town, South Africa, E-mail: rberndt@csir.co.za; W.A.J. Nel is with the with Council for Scientific and Industrial Research, Pretoria, South Africa, E-mail: wajnel@csir.co.za; M.Y. Abdul Gaffar and D.W. O'Hagan are with the Department of Electrical Engineering, University of Cape Town, Cape Town, South Africa, E-mail: (yunus.abdulgaffar@uct.ac.za; daniel.ohagan@fhr.fraunhofer.de); Corresponding author: R.J. Berndt.

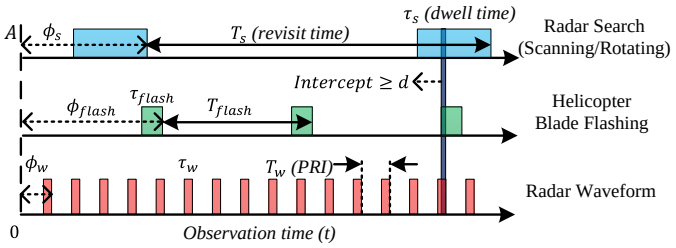

Fig. 1. Periodic processes, modeled as pulse trains, involved in the interception of helicopter blade flashes. The pulse train periods (T), pulse widths (τ) and start phases (ϕ) are indicated.

applicable to radars with constant sector revisit time. For mechanically scanned radars that scan back and forth within an angular sector, the analysis will only be relevant when the helicopter is situated precisely in the middle of the scan sector. The starting phases are assumed to be unknown, and uniformly distributed. Given that they are related to initial conditions at start-up, and the time of start-up relative to the start of the observation period (t), this is a reasonable assumption.

The aim of the analysis is to determine the Probability of Intercept (PoI) of at least one blade flash, after the pulse trains have been observed for a certain time t. These problems arise in the field of Electronic Support (ES), where ES receivers are required to intercept a scanning radar transmission while measuring at the correct frequency band. The nature of the problem has meant that there are a number of works that use reasonable approximations [16]–[18]. Clarkson [19]–[21] has also published extensively on this topic, and does not specifically rely on the use of approximations. The analysis in this paper draws significantly on this work.

The vertical dark blue region in Fig. 1 represents an interception event between the pulse trains. The parameter d defines the minimum duration an intercept must exist for to be valid. If $d = 0$, pulses only need to touch, while if $d = min(\tau_s, \tau_{flash}, \tau_w)$, the shortest of the pulses must overlap entirely with the others. d will have a very important influence on radar detection since it determines how much energy is returned to the radar. At closer ranges, a low d value might be sufficient to ensure detection, while longer ranges may require a higher value for d. As a compromise, for the remainder of the paper, it is assumed that $d = \tau_{min}/2$, where τ_{min} is the shortest pulse length of all the pulse trains under consideration.

Before proceeding, typical parameter values for helicopters and radars that relate to the analysis will be briefly discussed. Although 2, 3, 4 and 5 bladed helicopters are common, 2 bladed helicopters produce the lowest flash rate, and therefore represent a worst-case scenario for interception. Consequently, they are the main focus of this paper. The main rotor rotation rate for most helicopters lies between 250 and 500 Revolutions per Minute (RPM). This analysis focuses on the region between 350 to 450 RPM.

The analysis is performed for radars operating between 1 and 10 GHz, which includes a significant portion of typical search radars. Azimuth beamwidths for these radars vary roughly between 1° and 5 °. Search radars have pulse widths

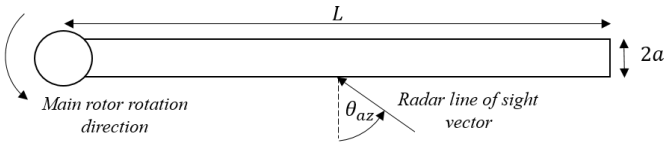

Fig. 2. Top view of a simplistic helicopter main rotor blade.

that can be roughly between 1μs and 100μs. In this paper a fairly conservative (i.e. longer) value is obtained by using 10% duty-cycle waveforms. The PRFs covered are between 1 and 15 kHz which extend slightly higher than is typical for search radars. Larger, longer range search radars typically have rotation rates between around 5 RPM and 30 RPM. Smaller, shorter range radars can have higher rotation rates of around 60 RPM. This study makes use of 15, 30 and 60 RPM.

III. Helicopter Main Rotor Blade Flashing

In this paper, simple models are used to provide equations for blade flash width and blade flash period that describe a pulse train. These are presented in the sections that follow.

A. Blade Flash Width

The Radar Cross Section (RCS) of helicopter blades, denoted by σ, can be approximated by modeling them as perfect electrical conducting cylinders. Using physical optics [22], the Equation for the RCS is

$$\sigma = kaL^2 \cos^2\theta_{az} \left[\frac{sin(kLcos(\theta_{el})sin(\theta_{az}))}{kLcos(\theta_{el})sin(\theta_{az})}\right]^2, \quad (1)$$

where $k = 2\pi/\lambda$, a is the cylinder radius, L is the length, θ_{az} is the angle off broadside as shown in Fig. 2, and θ_{el} is the elevation angle relative to the radar. Given the ranges at which radar targets are typically measured, θ_{el} is assumed to be small and reasonably approximated as 0°.

Using Equation 1, it can be shown that the null-to-null azimuth angular width of the flash is $\theta_{nn} \approx 2\pi/(kL)$. According to the Rayleigh resolution criterion, the angular width (α) of a 'sinc' type beam can be approximated as half the null-to-null width, yielding $\alpha \approx \lambda/(2L)$. The blade flash width in time (τ_{flash}) can then be calculated using the rotor rotation rate and expressed in terms of the blade tip speed. For even bladed helicopters the effective blade length can be considered to be twice that of a single blade, yielding the following approximations,

$$\tau_{flash} \approx \begin{cases} \frac{\lambda}{4v_{tip}} & \text{for} \quad N\ even \\ \frac{\lambda}{2v_{tip}} & \text{for} \quad N\ odd \end{cases}, \quad (2)$$

where N is the number of main rotor blades. In helicopters, due to aerodynamic considerations, the blade tip velocity must be kept roughly constant and generally falls between 200 to 250 m/s [3], [5], [9]. This constraint allows τ_{flash} to be specified independently of the rotor rotation rate and blade length, making it only a function of radar wavelength. For simplicity, Equation 2, with $v_{tip} = 225m/s$ was used to calculate τ_{flash} for the remainder of the results presented in this paper.

B. Blade Flash Period

The blade flash period (T_{flash}) is the other main parameter of interest for PoI analysis. It is calculated using Equation 3 below. f_{heli} is the main rotor rotation rate in Hz.

$$T_{flash} = \begin{cases} \frac{1}{f_{heli}N} & \text{for} \quad N \ even \\ \frac{1}{f_{heli}2N} & \text{for} \quad N \ odd \end{cases} \tag{3}$$

The equation entails that two blade flashes occurring simultaneously, as is the case for an even bladed helicopter, can be considered to be a single flash event.

C. Limitations

Some caveats of using some simplifying assumptions and basic models, such as those specified in the previous sections, merit a brief discussion:

- Maneuvering or accelerating helicopters can produce elevation angles that violate the small angle approximation previously stated. Larger elevation angles will lead to a broadening of the blade flashes in time that is not accounted for in this study.
- As noted by Point [7], the blade flash durations produced by a simple model such as Equation 2 can produce flash durations that are sometimes significantly less than have been observed in measured data. The difference is attributed to various deformations that the blades undergo when in motion.
- Receding and incoming flash durations may be different due to the different deformations the blades undergo.
- For even bladed helicopters, receding and incoming flashes may not occur simultaneously as is assumed in Equations 2 and 3.

As outlined above, there are scenarios in which the models and assumptions used in this study are inaccurate. The parameter values used however tend to err in a conservative direction, placing more stringent requirements on radar parameters than may be absolutely necessary. The work can thus be considered to provide lower bound estimates on the PoI of blade flashes.

IV. Single Pulse Train Probability of Interception

The continuous observation of a single pulse train over a period of time is illustrated in Fig. 3. The red region represents the observation time (t), and d the required overlap for an intercept to be legitimate. If $d = 0$, $P_{int}(t)$ can be viewed as the portion of T that has been observed (t), plus the pulse width, normalized by T. If the pulse train is observed for a single instant in time, $P_{int}(0) = \tau/T$. This takes into account all possible uniformly distributed pulse train start phases (ϕ).

Should $d > 0$, d must be subtracted from both τ and the observation time t to produce the correct probability. For $t > d$, Equation 4 expresses this mathematically.

$$P_{int}(t) = \frac{t + \tau - 2d}{T} \tag{4}$$

Once the pulse train has been observed for $t \geq T - \tau + 2d$, interception is certain since there is no possible region within the pulse period that could contain a pulse that has not been observed for the requisite duration. For pulse trains with $\tau \ll T$, the PoI progression over time is almost entirely dependent on the period (T).

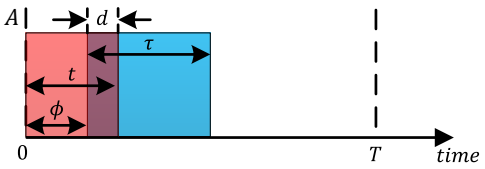

Fig. 3. PoI for one pulse train after an observation time t and a required overlap of d.

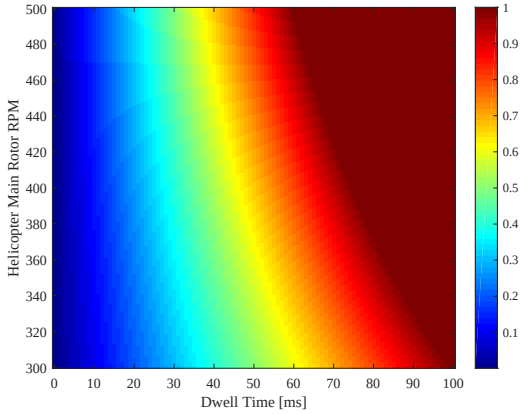

Fig. 4. Probability of main rotor blade flash intercept for at least one main rotor blade flash for two bladed helicopters at 10 GHz.

A. The Effect of Dwell Time on Target

When a helicopter is illuminated by a radar beam continuously (as is the case in a tracking radar), the probability of intercepting a blade flash over time can be calculated by applying Equation 4 with the relevant blade flash pulse train parameters.

Fig. 4 shows $P_{int}(t)$ for hypothetical two-bladed helicopters with different rotation rates, measured at 10 GHz as a function of dwell time. In generating the results, at least 50% of a blade flash must be observed to count as an intercept (i.e. $d = 0.5\tau_{flash}$). A dwell time greater than approximately 80 ms is required to guarantee intercept for most feasible main rotor rotation rates.

Although the results in Fig. 4 are generated for a specific transmit frequency, it is typical that $t \gg \tau_{flash}$. Taking this into account allows Equation 4 to be approximated as $P_{int}(t) \approx t/T_{flash}$, which is independent of radar transmit frequency. Consequently, the result in Fig. 4 can be considered largely independent of transmit frequency.

B. The Effect of PRF

The minimum requirement on PRF to guarantee blade flash interception can be analyzed in a similar manner to dwell time using Equation 4. The main difference is that the pulse train under consideration is not that of the blade flashing,

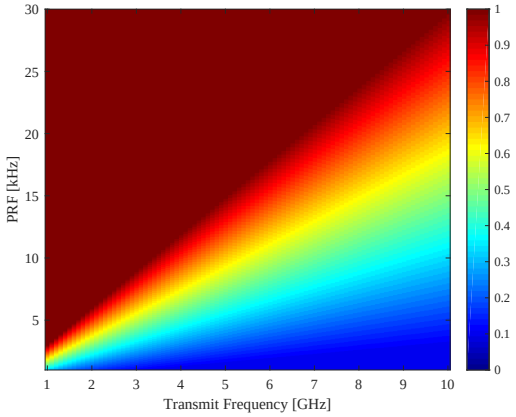

Fig. 5. Probability of main rotor blade flash intercept for two bladed helicopters after an observation time equal to one blade flash width.

but that of the radar waveform. For a waveform with a pulse repetition interval (T_w) and a transmitted pulse width (τ_w), the probability of interception can be evaluated for $t \leq \tau_{flash}$. In effect, a blade flash can be considered to 'observe' a waveform period.

Fig. 5 shows the $P_{int}(t)$ for different PRF and transmit frequency combinations after one completed blade flash ($t = \tau_{flash}$). The simulated radar transmit waveforms have a duty-cycle of 10%. It can be seen that to ensure intercept, a PRF that would be considered high[1] in the context of the transmit frequency is required.

V. Two pulse Train Probability of Interception

If the minimum requirements for interception in the previous section cannot be met (likely due to update rate requirements for target detection and tracking in search radar, or an unambiguous range requirement on the PRF), the problem becomes one concerned with the PoI of two pulse trains. One of these is produced by blade flashing, the other by a search radar antenna, or by the transmitted waveform of a pulse-Doppler radar.

Two variations of the PoI problem are analyzed here:

1) In the discrete time variation, as referred to by Clarkson [20], the PoI as a function of continuous observation time, $P_{int}(t)$, is determined for the case where the start phase of one of the pulse trains (call it pulse train 1) is known and the other (pulse train 2) is unknown and uniformly distributed over the period T_2. The obvious limitation here is that a random start phase of pulse train 1 (ϕ_1) is not accounted for. As will be explained in more detail in the next section, this limitation can be mitigated by only evaluating $P_{int}(t)$ (as derived for a particular ϕ_1 value) at non-zero integer multiples of T_1. At these time instants $P_{int}(t)$ is independent of ϕ_1 and is the reason for the 'discrete time' name for this variation of the problem. The analysis of this version is performed to help build a conceptual understanding and as an intermediate step towards the continuous time variation.
2) In the continuous time variations, both start phases are unknown and uniformly distributed over the respective pulse periods. The derived $P_{int}(t)$ is applicable for any continuous observation time t. Understanding of this variation is important as a foundation for the three pulse train PoI problem.

The analysis in the subsections that follow makes use of the following conventions:

- For the sake of brevity, it is always assumed that $T_1 \geq T_2$. It is, however, possible to perform the same analysis when $T_1 < T_2$. The outcomes and conclusions reached will be equivalent.
- It is assumed that the required overlap for an interception to be declared (as shown in Fig. 1 as d) has been accounted for in the pulse widths of each of the pulse trains (i.e. $\tau_i := \tau_i - d$). Consequently, the analysis can proceed as if the pulses are just required to touch to constitute an intercept.

A. Discrete Time PoI

Building on the explanation for a single pulse train (see Section IV), consider a hypothetical 2 pulse train scenario shown in Fig. 6. For illustration purposes, $\phi_1 = 0$, ϕ_2 is uniformly distributed over T_2 and the observation time is $2T_1$. Two examples of pulse train 2, with different start phases, are provided in red and gray. Similarly to Section IV, pulses from pulse train 1 can be considered to observe different portions of T_2. This is shown at the bottom of Fig. 6 where the blue and green pulses from pulse train 1 occupy different regions of T_2. Note that τ_2 is appended (or prepended depending on convention) to every observed region to fully account for all interception possibilities. With wrapping of the observed regions allowed, the total region covered is independent of ϕ_2. The average PoI over all possible ϕ_2 values is the total portion of T_2 that has been observed, normalized by T_2,

$$P_{int}(2T_1) = \frac{2(\tau_1 + \tau_2)}{T_2}. \tag{5}$$

While the process of observing the T_2 phase space can be used to account for the uniform distribution of ϕ_2, it does not account for a uniformly distributed ϕ_1. To illustrate this consider Fig. 7 which shows color-coded $P_{int}(t)$ curves for different ϕ_1 values. The different start phases produce unique $P_{int}(t)$ curves, however in all cases $P_{int}(T_1)$ is equal, independent of ϕ_1. This is generally true over extended observation times as long as $P_{int}(t)$ is evaluated at non-zero integer multiples of T_1. This is because, at these time instants, the total duration of observed τ_1 pulses (including partial pulses at the beginning and end of a period) is constant regardless of the start phase.

The discrete time version of the two pulse train problem is useful to analyze to develop an understanding of the influence of pulse widths and periods on the progression of PoI over time. This will be done in the two subsections that follow.

[1]likely range ambiguous and Doppler unambiguous

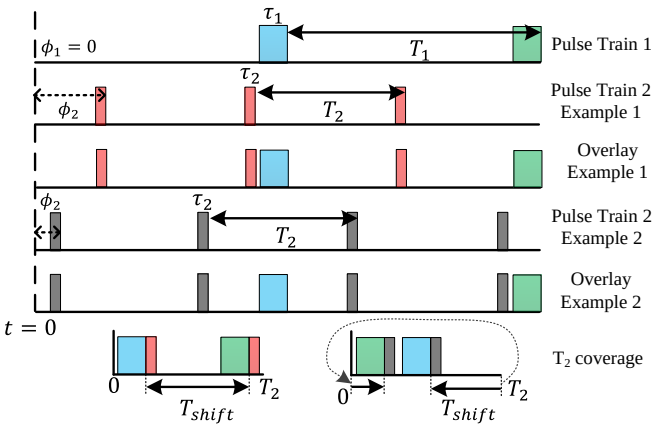

Fig. 6. PoI of 2 hypothetical pulse trains after $t = 2T_1$. The start phase of pulse train 2 is uniformly distributed and two examples (in red and gray) of start phases are provided.

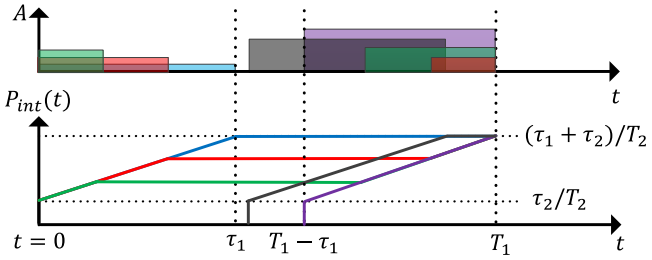

Fig. 7. Examples of the progression of the PoI over time for different values of ϕ_1, assuming ϕ_2 is uniformly distributed over T_2. The differing amplitudes of the pulses in the top graph have no significance and are varied purely for visibility reasons.

1) The Influence of Pulse Train Periods: To analyze the influence of pulse train periods, consider the parameter T_{shift}, as defined in the equation below, and indicated at the bottom of Fig. 6.

$$T_{shift} = \left(\frac{T_1}{T_2} - \left\lfloor \frac{T_1}{T_2} \right\rfloor \right) T_2 \tag{6}$$

Here, $\lfloor . \rfloor$ denotes the floor operation. This parameter determines where in the T_2 phase space a new τ_1 pulse falls relative to the previous τ_1 pulse. It thus influences how the PoI grows over time. If $0 < T_{shift} < \tau_1 + \tau_2$, successive τ_1 pulses 'observe' different parts of the T_2 phase space, however, at a decreased rate due to overlapping with previously observed regions. In the extreme, the PoI does not grow after the first τ_1 pulse. This occurs when there is persistent, complete overlap with previously observed regions of the T_2 phase space (i.e. $T_{shift} = 0$ since T_2 is an integer multiple of T_1). If the magnitude of T_{shift} is precisely one half of the T_2, every second scan will be observing the same portion of the T_2. Alternatively, if $T_{shift} = \tau_1 + \tau_2$, the PoI will grow to 1 at a maximum rate since each new τ_1 pulse observes a new region of T_2.

T_{shift} can assume any value between 0 and T_2, each of which provide a different way in which the T_2 phase space is observed over time. If T_{shift} is rational, there exists integers n and m, such that $nT_1 = mT_2$. The implication is that there is a point in time (t_r) that is a non-zero integer multiple of both T_1 and T_2. This is significant for the PoI because it means that from t_r onwards, no new regions of T_2 will be observed as the observation cycle will repeat indefinitely at integer multiples of t_r.

If T_{shift} is normalized by T_2 to produce $\tilde{T}_{shift}$, then $0 \leq \tilde{T}_{shift} < 1$ and rational $\tilde{T}_{shift}$ values are part of a set of fractions called Farey sequences [20] of a particular order. For example, the Farey sequences of order 1 and 2 are given by $F(1) = \left\{ \frac{0}{1} \frac{1}{1} \right\}$ and $F(2) = \left\{ \frac{0}{1} \frac{1}{2} \frac{1}{1} \right\}$. The selection of the appropriate order of Farey sequence for a particular pulse train interception problem will be addressed in the next section.

If T_{shift} is irrational, it is guaranteed that exactly the same point in the T_2 phase space will never be revisited. This has the benefit that the PoI will eventually grow to 1.

2) The Influence of Pulse Widths: From the example in Fig. 6, it is clear that in addition to the pulse periods, the length of both the pulses play a role in determining the growth of the PoI over time. When there is no overlap between new τ_1 pulses and previously observed portions of T_2, the probability grows at its maximum rate, which is $\Delta P_{int} = (\tau_1 + \tau_2)/T_2$.

The pulse widths also determine the order of Farey sequence (n_{farey}) applicable to a PoI problem. If $0 < \tilde{T}_{shift} \leq (\tau_1 + \tau_2)/T_2$ and rational (i.e. a member of a Farey sequence), new 'observations' from τ_1 pulses will always overlap with the previous one. This means that there cannot be regions in T_2 that are unobserved by the time the 'observation cycle' starts to repeat. The appropriate order of Farey sequence should therefore not contain any values $< (\tau_1 + \tau_2)/T_2$. The equation to determine n_{farey} is given below [20],

$$n_{farey} = \left\lceil \frac{T_2}{\tau_1 + \tau_2} \right\rceil - 1, \tag{7}$$

where $\lceil . \rceil$ denotes the ceiling operation. The number of Farey sequence values in a set grows with increasing order. Consequently, the lower the order, the lower the possibility that $\tilde{T}_{shift}$ will fall on or close to a Farey sequence number. Given Equation 7, it is clear that the larger $\tau_1 + \tau_2$ is, the better. If $\tilde{T}_{shift} > (\tau_1 + \tau_2)/T_2$ and is a Farey sequence value, it is possible but not certain, that the PoI 'saturates' before reaching 1. This will occur because observed regions within the T_2 phase space are revisited repeatedly, while unobserved regions remain as such. T_2 can never therefore be fully observed and the PoI converges to a value < 1.

3) PoI Calculation: A conceptually simple algorithm to calculate the PoI after a certain number of T_1 periods can be conceived with reference to the example in Fig. 6. The algorithm keeps track of the regions of T_2 observed after every T_1 period (including the merging of any overlapping regions). The PoI can then be calculated by summing the length of the regions covered and normalizing by T_2. While such an algorithm is straightforward to implement, it is not necessarily computationally efficient.

In [20], Clarkson derives a piecewise linear equation to solve this problem that is significantly more efficient than the approach discussed above. Exploiting the same principles discussed in the previous two sections, the equation makes use of outputs from the Simple Continued Fraction (SCF) expansion

of the ratio of the pulse periods. The approximation tolerance that is used as a stopping criterion for the SCF expansion is set to the sum of the pulse widths. The resulting equation consists of 4 linear segments. The slope of the segments and their boundaries are determined by the pulse train parameters and the outputs (some of which are intermediate) from the SCF expansion.

B. Continuous Time PoI

For the continuous time problem, uncertainty in phase for both pulse trains must be taken into account to produce a PoI at any observation time $t >= 0$. To investigate the effect of a uniformly distributed ϕ_1, consider the ensemble of functions $P_{int}(t, \phi_1)$. Several examples of such functions are shown by the colored plots at the bottom of Fig. 7. Each of the functions is produced by observing the coverage of the T_2 phase space over time for a particular ϕ_1 value in the interval $[0, T_1)$.

Since $P_{int}(t, \phi_1)$ is a function of the uniformly distributed random variable ϕ_1, it can be considered a stochastic process, the average of which can be calculated as follows,

$$\overline{P_{int}(t)} = \frac{1}{T_1} \int_0^{T_1} P_{int}(t, \phi_1)\ d\phi_1, \tag{8}$$

The computational requirements to numerically solve Equation 8 can be reduced significantly by exploiting the behavior of $P_{int}(t, \phi_1)$ over time for $\phi_1 \in [\tau_1, T_1)$. To show this, $\overline{P_{int}(t)}$ can be expressed as the summation of two terms:

$$\overline{P_{int}(t)} = \frac{\tau_1}{T_1} \overline{P_{int}(t)}_{\phi_1 \in [0, \tau_1)} + \frac{T_1 - \tau_1}{T_1} \overline{P_{int}(t)}_{\phi_1 \in [\tau_1, T_1)} \tag{9}$$

For the first term in Equation 9, the τ_1 pulse is only partially present at $t = 0$. In Fig. 7, examples of functions that fall in this interval are colored green and red. Each of the functions in this interval have unique probability progressions over time. Calculating $\overline{P_{int}(t)}_{\phi_1 \in [0, \tau_1)}$ involves averaging all the unique $P_{int}(t, \phi_1)$ curves for all applicable values of ϕ_1.

The calculation of $\overline{P_{int}(t)}_{\phi_1 \in [\tau_1, T_1)}$ can proceed slightly differently. When $\phi_1 \in [\tau_1, T_1)$, no partial τ_1 pulse is encountered, and different values of ϕ_1 in this interval produce the same probability progression over time, except for a time delay. Examples of this are shown in Fig. 7 as the blue, gray and purple colored curves. Expressed mathematically,

$$P_{int}(t, \tau_1 + \Delta t) = P_{int}(t - \Delta t, \tau_1), \tag{10}$$

provided $\Delta t \in [0, T_1 - \tau_1]$. $\overline{P_{int}(t)}_{\phi_1 \in [\tau_1, T_1)}$ can then be determined by averaging delayed versions of $P_{int}(t, \tau_1)$ up to a delay of $T_1 - \tau_1$, as expressed in Equation 11 where β is a dummy integration variable.

$$\overline{P_{int}(t)}_{\phi_1 \in [\tau_1, T_1)} = \frac{1}{T_1 - \tau_1} \int_0^{T_1 - \tau_1} P_{int}(t - \beta, \tau_1)\ d\beta \tag{11}$$

For numerical computation, producing an accurate estimate of $\overline{P_{int}(t)}_{\phi_1 \in [\tau_1, T_1)}$ in Equation 11 entails that $P_{int}(t, \tau_1)$ is known for a sufficient number of uniformly distributed values of t over an interval of at least $T_1 - \tau_1$. This requirement is less computationally intensive than having to simulate $P_{int}(t, \phi_1)$ for all $\phi_1 \in [\tau_1, T_1]$ at only a single time value (which is when the computational saving is at its lowest). This is because the operations required to compute $P_{int}(t, \tau_1)$ for later values of t require the same operations already completed for earlier values of t. For all $\phi_1 \in [\tau_1, T_1]$ at one value of t, they are independent.

By exploiting Equation 11, the number of computations required to calculate $\overline{P_{int}(t)}$ can be reduced by a factor close to $(T_1 - \tau_1)/T_1$. Given that often $\tau_1 \ll T_1$, this can be a significant saving.

As with the discrete time problem, Clarkson has also analyzed the continuous time problem and produced an expression for the PoI over time [19], [20]. The expression is very similar to the discrete time expression as it is also piecewise linear. There is, however, an additional quadratic segment. The simulation results presented in Sections V-C and V-D are generated using this expression [20]. This was done for reasons of accuracy and efficiency. The detailed analysis in this section is provided to develop a conceptual understanding and to build towards an algorithm for three pulse train PoI problems, which Clarkson's expression does not cater for. This will be covered in Section VI.

C. The Effect of Radar Scanning

The parameters of a pulse train formed by a rotating radar antenna can be calculated using the antenna rotation rate (f_s) and the radar antenna azimuth beamwidth (B_{az}). The period (T_s) is given by $T_s = 1/f_s$, where f_s is in Hz. The dwell time on target (τ_s) for each rotation is $\tau_s = B_{az}/(360 f_s)$, for B_{az} in degrees.

Fig. 8 shows the PoI and a function of time for hypothetical two-bladed helicopters with rotation rates between 350 and 450 RPM. For each of the three plots in the figure the radar azimuth beamwidth is set to 2.5° with the scan rate being 15, 30, and 60 RPM. In each of the plots, the growth in probability over time is evident. The most prominent features are the helicopter RPM values that result in Farey sequence points. They can be seen as valleys in the probability surfaces that extend over time. They are increasingly prevalent and deeper for high radar scan rates. This is to be expected given Equation 7 from Section V-A2. The higher the antenna rotation rate, the higher the applicable order of Farey sequence and thus the number of Farey sequence values.

To quantify the influence of different antenna rotation rates and beamwidths, probabilities are averaged over helicopter rotation rates, however, the transmit frequency is kept constant at 9 GHz. Resulting average probability curves are presented in Fig. 9 for observation times of 4 and 15 seconds. At 4 seconds, there is a notable difference between performance at 15 RPM compared to the others. This is the result of the antenna rotation rate and beamwidth combinations guaranteeing flash intercept in a single dwell for a higher proportion, and in some cases all, of the simulated helicopter rotation rates (350 - 450 RPM).

It is clear that unless the antenna rotation rate is low enough to guarantee intercept, it plays a fairly insignificant role in the development of the PoI over time. Beamwidth is

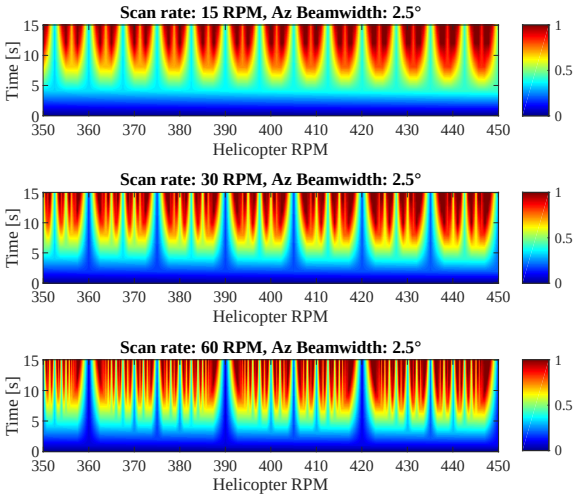

Fig. 8. PoI for hypothetical two bladed helicopters as a function of time and helicopter rotation rate for radar rotation rates of 15 RPM, 30 RPM and 60 RPM. Radar transmit frequency is 9 GHz and the radar antenna azimuth beamwidth is 2.5°.

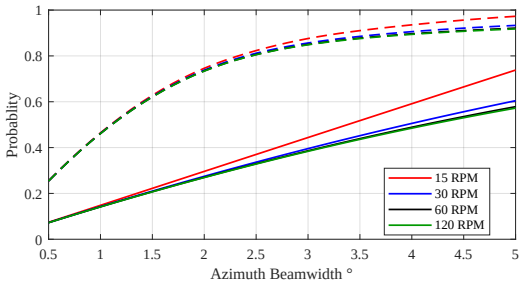

Fig. 9. PoI for two bladed helicopters as a function of azimuth beamwidth for different antenna rotation rates, after 4 (solid line) and 15 (dashed line) second observation times. The radar transmit frequency is 9 GHz.

significantly more important. A plausible explanation for this is that the decreased PoI associated with a shorter dwell (or higher antenna rotation rate) is counteracted to a large extent by an improved update rate.

By the time 15 seconds have elapsed the difference in performance between rotation rates is negligible. It is clear that, for shorter observation times, there is significant benefit to ensuring that a single dwell intercept is guaranteed. Relying on multiple revisits to improve the PoI is effective, but comes at the cost of the observation time required.

Fig. 8 and Fig. 9 also highlights an important practical observation. To provide an indication of PoI levels that can be expected on average, the results in Fig. 9, and in almost all of the results that follow in this paper, are the average over likely helicopter main rotor RPMs. Fig. 8 shows that the performance obtained for a particular helicopter can vary significantly from the average. Even though average PoI performance may be acceptable, the performance for a particular helicopter may not be. The simplifying independence assumptions often used to calculate the cumulative PoI after multiple scans [9], [14] do not provide this insight. It is worth noting that although results in Fig. 9 are produced for 9 GHz, they are relatively insensitive to transmit frequency.

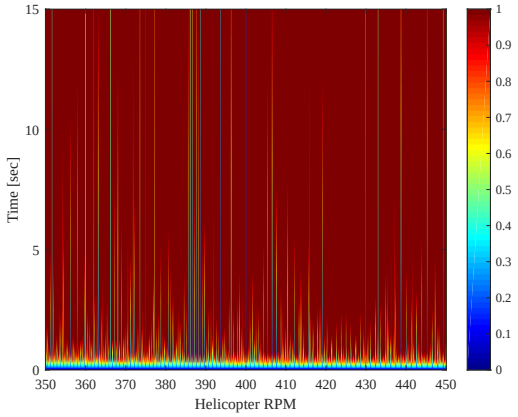

Fig. 10. PoI as a function of time for hypothetical two bladed helicopters with rotation rates between 350 and 450 RPM. The PRF is 5 kHz, waveform duty-cycle 10% and the transmit frequency is 9 GHz.

D. The Effect of Radar Waveform

The effect of a PRF that is too low will now be considered. It is assumed in this section that the target is being observed continuously (i.e. no antenna scanning). Fig. 10 shows the PoI as a function of time for hypothetical two-bladed helicopters. There is a strong prevalence of helicopter RPMs that are Farey sequence values as evidenced by the numerous valleys in the probability surface extending vertically over time. It is however noticeable that the majority of helicopter RPM values have a high PoI after about a second. This is significantly shorter than what was seen for the radar scanning in the previous section and is to be expected given the comparatively shorter pulse periods.

Fig. 11 presents the average PoI at observation times of 0.1s and 0.5s for hypothetical helicopters with rotation rates between 350 and 450 RPM at different PRF and transmit frequencies. The waveform duty-cycle is kept constant at 10%. At an observation time of 0.1s, all the simulated helicopter flash periods have elapsed. As a result, all PRF-transmit frequency combinations that guarantee intercept after 1 flash are at a probability of 1. As with radar scanning, it is evident that time does cause an improvement in probability levels as there is significant growth in PoI after only 0.5s. Given the fast initial growth, the extent of the improvement is not significant after an extended observation period.

It is interesting to note that for a 10 GHz transmit frequency, at PRFs below 3 kHz the PoI appears to no longer be dependent on PRF. Likewise, at 6 GHz, PRFs below 1.8 kHz no longer influence the PoI. The reason for this relates to the definition of the required overlap for interception (d). At the respective transmit frequencies, PRFs below 3 kHz and 1.8 kHz result in $\tau_w > \tau_{flash}$. Recall from Section II that, $d = 0.5[min(\tau_w, \tau_{flash})]$, thus $d = 0.5\tau_{flash}$ in this case. As highlighted in Section V-A2, $\tau_1 + \tau_2$ plays a critical in the growth of the PoI. For these PRFs, $\tau_w + \tau_{flash} - 2d = \tau_w$ and the growth of the PoI is effectively independent of τ_{flash}. Because a fixed duty-cycle waveform is used, as T_w grows, so does τ_w in the same proportion. When averaged over the

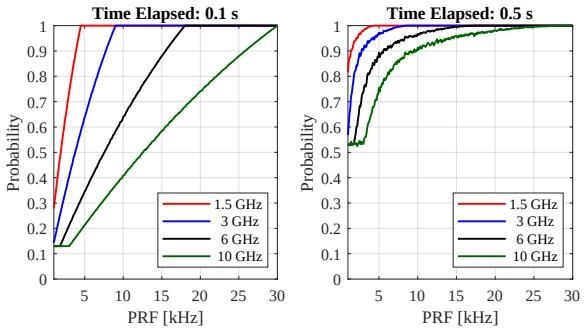

Fig. 11. Averaged probability of main rotor blade flash intercept for at least one main rotor blade flash for two bladed helicopters for differing PRFs and transmit frequencies after observation times of 0.1 and 0.5 s. The helicopter rotation rates over which the PoI is averaged are uniformly distributed between 350 and 450 RPM and the waveform duty-cycle is 10%.

different simulated helicopter flash rates, this results in the constant PoI that is observed.

VI. Three Pulse Train Probability of Interception

When the requirements to guarantee intercept for radar waveform (i.e. PRF) and radar scanning (i.e. too short dwell time) are simultaneously unmet, a three pulse train PoI problem is encountered as shown in Fig. 1. The PoI for more than two pulse trains becomes increasingly difficult to solve. Clarkson has shown in [20] that, for such a problem, the number of linear segments in an expression for the PoI over time is unbounded. Consequently, it is not possible to derive an expression as was done for the discrete and continuous time two pulse train problems. Clarkson then resorts to considering only short observation times, where it is possible to derive exact expressions for M pulse trains. The approximation developed by Self and Smith [18], which is also applicable to M pulse trains, suffers from the same problem of only being accurate for short observation time periods.

The approach to calculate the three pulse train PoI in this paper can be considered an extension of the continuous time two pulse train algorithm from Section V-B. It combines Monte Carlo simulation with statistical analysis to produce an algorithm that is accurate and more efficient than pure Monte Carlo.

Assume that the pulse trains are ordered by period length such that labels 1, 2, and 3 result in $T_1 \geq T_2 \geq T_3$. For illustration, assume that start phases ϕ_1 and ϕ_3 are set to constant values. Such a scenario is shown in Fig. 12. The first step in calculating the PoI involves determining the overlapping regions between pulse trains 1 and 3. Together they form a new merged pulse train, possibly with an irregular period and pulse width (the purple regions in Fig. 12). The merged pulse train then 'observes' the T_2 phase space as described in previous sections. Again, τ_2 is appended to every observed region and wrapping is allowed. A single probability curve as a function of time, $P_{int}(t, \phi_1, \phi_3)$, can then be determined. To produce the average probability curve for all start phases,

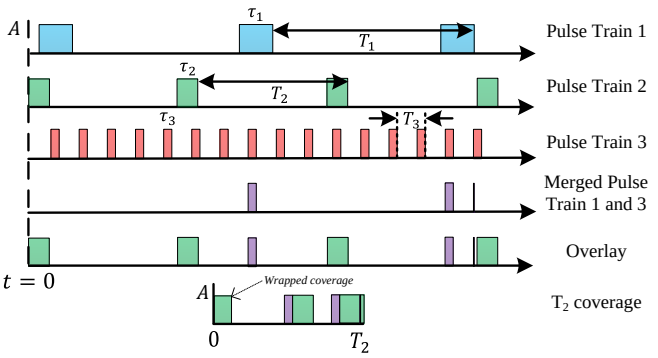

Fig. 12. Example of the calculation of the PoI for 3 hypothetical pulse trains. The start phase of pulse train 1 and 3 are known.

the same procedure must be repeated for all $\phi_1 \in [0, T_1)$ and $\phi_3 \in [0, T_3)$, and the results averaged.

$$\overline{P_{int}(t)} = \frac{1}{T_1 T_3} \int_0^{T_1} \int_0^{T_3} P_{int}(t, \phi_1, \phi_3)\ d\phi_1\ d\phi_3. \quad (12)$$

Numerically, this entails sampling ϕ_1 and ϕ_3 at a fine enough resolution or using Monte Carlo simulation. Just as for the continuous time two pulse problem, an improvement in efficiency is possible. The first step is to take ϕ_3 into account over $[0, T_3)$ to produce,

$$\overline{P_{int}(t, \phi_1)} = \frac{1}{T_3} \int_0^{T_3} P_{int}(t, \phi_1, \phi_3)\ d\phi_3. \quad (13)$$

$\overline{P_{int}(t, \phi_1)}$ represents an ensemble of curves, each of which is produced by a different ϕ_1 value and the average of $\phi_3 \in [0, T_3)$. The desired average probability can then be specified by breaking it into two terms.

$$\overline{P_{int}(t)} = \frac{1}{T_1} \left(\int_0^{\tau_1} \overline{P_{int}(t, \phi_1)}\ d\phi_1 + \int_{\tau_1}^{T_1} \overline{P_{int}(t, \phi_1)}\ d\phi_1 \right). \quad (14)$$

The first term in Equation 14 must be calculated by averaging all the individual curves $\overline{P_{int}(t, \phi_1)}$ for $\phi_1 \in [0, \tau_1)$. The second term can be calculated differently to allow for computational efficiency as with the two pulse problem. For $\phi_1 \in [\tau_1, T_1)$, a change in ϕ_1 is equivalent to a shift in time, thus

$$\int_{\tau_1}^{T_1} \overline{P_{int}(t, \phi_1)}\ d\phi_1 = \int_0^{T_1 - \tau_1} \overline{P_{int}(t - \beta, \tau_1)}\ d\beta. \quad (15)$$

This means that ϕ_1 only needs to be varied in the interval $[0, \tau_1]$ during computation.

A. The Simultaneous Effect of Radar Waveform and Radar Scanning

The simultaneous effect of radar waveform and scanning was investigated using the algorithm described in the previous section. It was developed in Julia [23] to exploit the speed and distributed computing capability provided by the language. The simulation implementation was verified as follows:

1) The results match those produced by the exact expression from Clarkson [20], that is applicable only for short observation intervals.
2) A three pulse train problem with one pulse train having a 100% duty-cycle produced the same results as an equivalent two pulse train problem (i.e. the 100% duty-cycle pulse train can be removed). Thereafter, as the duty-cycle was shortened, the calculated probabilities decreased compared to those produced for the two pulse problem.

To generate results, the algorithm was deployed in parallel across multiple Central Processing Unit (CPU) cores, on multiple different machines in a High Performance Computing (HPC) Cluster. To account for the uniform start phases in each specific 3 pulse train interception problem, a Monte Carlo simulation was run for different combinations of $\phi_1 \in [0, \tau_1)$ and $\phi_3 \in [0, T_3)$ (see previous section for details). Each of the three pulse trains are specified by two parameters (pulse width and period, start phase is accounted for in the algorithm) making a total 6 of parameters. Simulating many variations of all these parameters results in a combinatorial explosion. For this reason, the extent to which each parameter could be varied had to be constrained as follows:

- Antenna beamwidth: 2.5° and 5°
- Antenna scan rate: 15, 30, and 60 RPM
- Transmit frequency: 1.5 GHz, 3 GHz, 6 GHz and 10 GHz
- Helicopter main rotor rotation rate: 401 values uniformly distributed between 350 and 450 RPM
- PRF: 1 kHz to 15 kHz in 200 Hz steps
- Waveform duty-cycle: Fixed at 10%

To illustrate the effect of radar scanning and waveform combined, Fig. 13 provides a comparison with related two pulse train results. Where PRF is relevant it is set to 5 kHz and the transmit frequency is 9 GHz. The addition of a third pulse train has a significant effect on the achieved probability. In both of the two pulse train results, a significant portion of the probability surface is equal to 1, whereas the three pulse train result does not reach levels more than roughly 0.3. To investigate this further, Fig. 14 provides the average PoI over helicopter main rotor rotation rates at observation times of 4 seconds (at least 1 full antenna rotation at the slowest antenna RPM), and 40 seconds. The left column provides results for a radar with an antenna azimuth beamwidth of 2.5°, and the right column provides results for a radar with an antenna azimuth beamwidth of 5°. Rows 1, 2, and 3 provide results for antenna rotation rates of 15, 30 and 60 RPM respectively. In all the sub-figures, PRFs greater than 4.5 kHz at 1.5 GHz, and greater than 9 kHz at 3 GHz represent scenarios where the PRF is high enough so that it no longer is a factor in interception. This region can be used as a reference for what is achievable when only scanning is relevant. In the two pulse train results in previous sections, there was clear benefit to specifying parameters such that only one scan or PRI was required for intercept. This kind of observation extends to the three pulse problem, where there is clear benefit to making it a two pulse train problem.

It is also evident that at PRFs lower than 3 kHz at 10 GHz

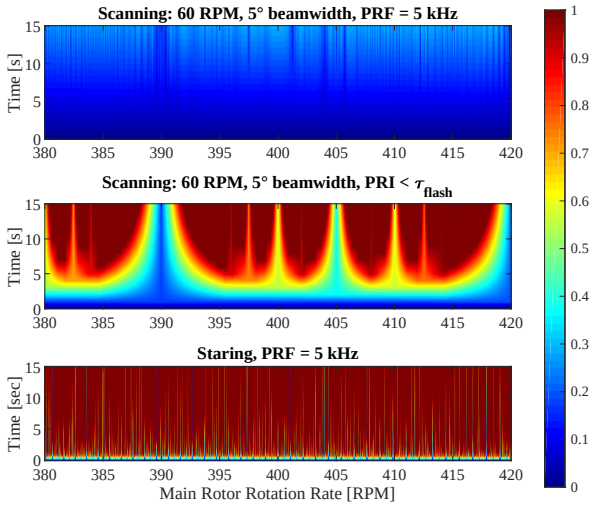

Fig. 13. Comparison between the PoI as a function of time and helicopter RPM for different measurement scenarios. Bottom: staring measurement of a helicopter at a PRF of 5 kHz (too low to guarantee interception). Middle: the PRF is high enough to guarantee intercept while the radar scans (dwell is too short to guarantee intercept). Top: the radar is scanning and the PRF is 5 kHz. The transmit frequency is 9 GHz and the hypothetical helicopters with different rotation rates are all 2 bladed.

and 1.8 kHz at 6 GHz, the same plateau in PoI as encountered in Section V-D is seen. This is again a consequence of the overlap parameter d as previously discussed.

The most dramatic affect on performance occurs during the initial period of observation. At 4 seconds, regardless of the radar rotation rate and beamwidth, there is a significant portion of the PRF-transmit frequency space that produce probabilities that are too low to be of practical use.

Comparing the results for the different antenna rotation rates, it can be seen that it is not influential at all. The antenna beamwidth once again has a more significant effect.

If length of observation is not a critical parameter to minimize, the PoI can be improved to be above 0.8 for a significant portion of the PRF-transmit frequency combinations. This is true even for the worst-case scan parameters of 60 RPM and 2.5° beamwidth. However, even after 40 seconds of observation, there remain lower PRF and higher transmit frequency combinations for which the PoI does not reach more than 0.8. Radars operating in this region cannot expect to produce any kind of reliable blade flash detection performance.

VII. Conclusion

The probability of helicopter main rotor blade flash intercept in scanning pulse-Doppler radar has been thoroughly analyzed in this paper. This work extends insight into blade flash detection, enabling more predictable and reliable target classification. To ensure that blade flashes are intercepted in a single dwell, dwell times greater than approximately 80 ms are required. PRFs greater than roughly $> 900/\lambda$ ensure interception by a pulsed radar waveform. When either or both of these two requirements are not met, relying on multiple pulses or scan revisits to improve the PoI can be effective. If the minimum requirement on dwell time is not met, antenna azimuth beamwidth plays a significant role in

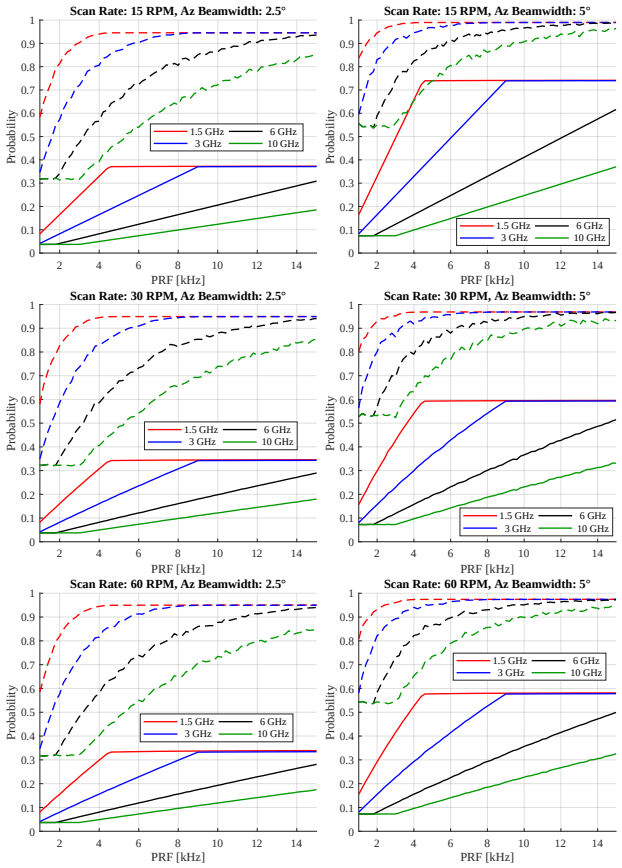

Fig. 14. Average PoI after an observation time of 4 seconds (solid lines) and 40 seconds (dashed lines) for hypothetical two bladed helicopters as a function of PRF at different radar antenna rotation rates, azimuth beamwidths and transmit frequencies. The probabilities are averaged over helicopter rotation rates between 350 and 450 RPM.

improving the growth of PoI over time. Scan rate is relatively inconsequential. When staring at a helicopter, if the PRF requirement is not met, a high PoI (> 0.8) is attained for a large number of PRF - transmit frequency combinations within roughly the first 1 second of observation. Thereafter, the rate of improvement diminishes significantly.

When dwell and PRF requirements are both unmet, PoI performance is particularly compromised during the initial phase of observation and a reasonably long period of time (> 15 seconds) is required if reasonable PoI levels (> 0.8) are to be attained. In general, it is advisable to ensure that intercepting blade flashes never becomes a three pulse train interception problem.

The results produced have focused on average probabilities, particularly for the worst-case, two-bladed helicopter scenario. For helicopters outside this category, the blade flash PoI may be significantly higher than that presented in this paper. It should also be noted, as highlighted in Section V-C, that PoI performance for individual helicopters can differ substantially from the average.

Acknowledgment

The authors would like to thank and acknowledge Reutech Radar Systems, Armscor, and the Council for Scientific and Industrial Research (CSIR) for contributing to the funding used to complete this study.

References

[1] H. Schneider, "Application of an autoregressive reflection model for the signal analysis of radar echoes from rotating objects," in *ICASSP-88., Int. Conf. Acoust. Speech, Signal Process.*, pp. 1236–1239, IEEE, 1988.

[2] J. Martin and B. Mulgrew, "Analysis of the theoretical radar return signal form aircraft propeller blades," in *IEEE Int. Conf. Radar*, pp. 569–572, IEEE, 1990.

[3] B. Bullard and P. Dowdy, "Pulse doppler signature of a rotary-wing aircraft," *IEEE Aerosp. Electron. Syst. Mag.*, vol. 6, pp. 28–30, May 1991.

[4] H. Green, "Electromagnetic backscattering from a helicopter rotor in the decametric wave band regime," *IEEE Trans. Antennas Propag.*, vol. 42, pp. 501–509, Apr. 1994.

[5] J. Misiurewicz, "Analysis of recorded helicopter echo," in *Radar Syst. (RADAR 97)*, vol. 1997, (Edinburgh), pp. 449–453, IEE, 1997.

[6] M. Burgos-Garcia, F. Perez-Martinez, and J. Gismero Menoyo, "Radar signature of a helicopter illuminated by a long lfm signal," *IEEE Trans. Aerosp. Electron. Syst.*, vol. 45, pp. 1104–1110, July 2009.

[7] G. Point and L. Savy, "Simple modelling of the radar signature of helicopters," in *Int. Conf. Radar Syst. (Radar 2017)*, no. 1, pp. 1–6, Institution of Engineering and Technology, 2017.

[8] A. G. Stove, "A doppler-based target classifier using linear discriminants and principal components," *High Resolut. Imaging Target Classif. 2006. Inst. Eng. Technol. Semin.*, pp. 107–125, 2006.

[9] J. Misiurewicz, K. S. Kulpa, Z. Czekala, and T. A. Filipek, "Radar detection of helicopters with application of clean method," *IEEE Trans. Aerosp. Electron. Syst.*, vol. 48, pp. 3525–3537, Oct. 2012.

[10] A. Cilliers and W. Nel, "Helicopter parameter extraction using joint time-frequency and tomographic techniques," in *2008 Int. Conf. Radar*, pp. 598–603, IEEE, Sept. 2008.

[11] S.-H. Yoon, B. Kim, and Y.-S. Kim, "Helicopter classification using time-frequency analysis," *Electron. Lett.*, vol. 36, no. 22, pp. 1871–1872, 2000.

[12] R. Melino, S. Kodituwakku, and H.-T. Tran, "Orthogonal matching pursuit and matched filter techniques for the imaging of rotating blades," in *2015 IEEE Radar Conf.*, no. 1, pp. 1–6, IEEE, Oct. 2015.

[13] S. T. N. Nguyen, S. Kodituwakku, R. Melino, and H.-T. Tran, "Wavelet-based sparse representation for helicopter main rotor blade radar backscatter signal separation," *IEEE Trans. Aerosp. Electron. Syst.*, vol. 53, pp. 2936–2949, Dec. 2017.

[14] P. Tait, *Introduction to Radar Target Recognition*. The Institution of Engineering and Technology, Michael Faraday House, Six Hills Way, Stevenage, UK: IET, Jan. 2005.

[15] V. C. Chen, *Radar Micro-Doppler Signature: Processing and Applications*. The Institution of Engineering and Technology, Michael Faraday House, Six Hills Way, Stevenage, UK: IET, May 2014.

[16] P. I. Richards, "Probability of coincidence for two periodically recurring events," *Ann. Math. Stat.*, vol. 19, no. 1, pp. 16–29, 1948.

[17] S. Stein and D. Johansen, "A statistical description of coincidences among random pulse trains," *Proc. IRE*, vol. 46, pp. 827–830, May 1958.

[18] A. Self and B. Smith, "Intercept time and its prediction," *IEE Proc. F Commun. Radar Signal Process.*, vol. 132, no. 4, pp. 215–220, 1985.

[19] I. V. L. Clarkson, J. Perkins, and I. Mareels, "Number/theoretic solutions to intercept time problems," *IEEE Trans. Inf. Theory*, vol. 42, pp. 959–971, May 1996.

[20] I. V. L. Clarkson, *Approximation of Linear Forms By Lattice Points*. PhD thesis, The Australian National University, 1997.

[21] I. V. L. Clarkson, "The arithmetic of receiver scheduling for electronic support," in *2003 IEEE Aerosp. Conf. Proc. (Cat. No.03TH8652)*, vol. 5, pp. 2049–2064, IEEE, 2003.

[22] T. J. Hestilow, "Simple formulas for the calculation of the average physical optics rcs of a cylinder and a flat plate over a symmetric window around broadside," *IEEE Antennas Propag. Mag.*, vol. 42, no. 5, pp. 48–52, 2000.

[23] J. Bezanson, A. Edelman, S. Karpinski, and V. B. Shah, "Julia: A fresh approach to numerical computing," *SIAM Rev.*, vol. 59, no. 1, pp. 65–98, 2017.

Robert John Berndt completed a BEng electronic engineering degree at the University of Pretoria, South Africa, in 2007. Since 2008 he has been with the Council for Industrial and Scientific Research (CSIR), Pretoria, South Africa, as a radar signals and systems analyst. At present his main fields of interest are radar signal processing, machine learning, and target recognition with a specific focus on micro-Doppler techniques. While at the CSIR he has completed his BEng (Honours) in electronic engineering at the University of Pretoria (2009) and is currently enrolled at the University of Cape Town, South Africa, where he is studying towards a Ph.D. degree in electrical engineering.

Wille Nel is a chief radar researcher at the CSIR in South Africa where he leads the Synthetic Aperture Radar group with a focus on the development of airborne, UAV and spaceborne SAR systems and is also appointed as the Technology and Innovation Manager for the radar area. He holds an MSc in Digital Image Processing from the University of Cape Town and a BEng in electronic engineering from the University of Pretoria. He has been working passionately in the field of radar since 1999, with a focus on radar system design, radar based target recognition, imaging radar and radar signal processing. He has published more than 30 research papers in radar target recognition and imaging and is the primary engineer behind several CSIR radar technology demonstrators. He is a IEEE senior member, is active within the IEEE AESS Radar Systems Panel and as a member and elected chair of the IEEE Dennis J. Picard Medal Committee.

Mohammed Yunus Abdul Gaffar received the B.Sc.Eng. and M.Sc.Eng. degrees in electronic engineering from the University of Natal, KwaZula-Natal, South Africa, in 2002 and 2003, respectively. He was with the Council for Scientific and Industrial Research (CSIR), Pretoria, South Africa, from 2003 to 2016, where he was active in the fields of inverse synthetic aperture radar and radar detection of ground moving objects. During his time at the CSIR he studied towards and received a Ph.D. degree in electrical engineering from the University of Cape Town, South Africa, in 2009. In 2016, he joined the University of Cape Town, as a Senior Lecturer. His research interests are in the fields of short-range radar systems and radar signal processing.

Daniel W. O'Hagan is Head of the Passive Radar and Anti-Jamming Techniques Department, Fraunhofer FHR, Wachtberg, Germany. His department consists of four groups focused on Passive and Networked Radar, Electronic Warfare, Advanced Concepts and System Development. He is an Honorary Professor at the University of Birmingham, U.K., affiliated with the Microwave Integrated Systems Laboratory (MISL). He is an Honorary Associate Professor in radar at the University of Cape Town (UCT) and former convener of the internationally renowned UCT Radar Masters Course. Daniel is Chair and DEU National Representative of NATO SET-268 "Bi-/Multi-static radar performance evaluation under synchronised conditions", Chair and DEU National Representative of NATO SET-296 on "Radar against Hypersonic Threats" and former Chair of SET-207, and SET-164. He is the recipient of the NATO SET Early Career Award in 2019. Daniel is Editor-in-Chief of the IEEE AESS Magazine and Associate Editor for Radar with the same publication. He has guest edited several specials issues of the IEEE AESS Magazine, the IET RSN Journal and the MDPI Sensors Journal. He contributes regularly to Technology Watch initiatives. Daniel has lectured at some of the leading R&D establishments throughout the world.